

Article

The Influence of Homogenisation Parameters on the Microstructure and Hardness of AlMnFeMgSi(Zr) Wrought Alloys

Jette Broer¹, Sina Mallow¹, Kevin Oldenburg², Benjamin Milkereit^{1,3}  and Olaf Kessler^{1,3,*} 

¹ Faculty of Mechanical Engineering and Marine Technology, University of Rostock, Albert-Einstein-Str. 25, 18059 Rostock, Germany; jette.broer@uni-rostock.de (J.B.); sina.mallow@uni-rostock.de (S.M.); benjamin.milkereit@uni-rostock.de (B.M.)

² Centre for Interdisciplinary Electron Microscopy (ELMI-MV), Department Life, Light & Matter, Faculty of Interdisciplinary Research, University of Rostock, Albert-Einstein-Str. 25, 18059 Rostock, Germany; kevin.oldenburg@uni-rostock.de

³ Competence Centre °CALOR, Department Life, Light & Matter, Faculty of Interdisciplinary Research, University of Rostock, Albert-Einstein-Str. 25, 18059 Rostock, Germany

* Correspondence: olaf.kessler@uni-rostock.de; Tel.: +49-381-498-9470

Abstract: The purpose of this investigation is to improve the mechanical properties of AlMnFeMgSi wrought alloys by forming a high number density of nano-scaled strengthening dispersoids during homogenisation annealing. The process chain for AlMnFeMgSi wrought alloys includes homogenisation annealing after continuous casting. In this step, inhomogeneities and segregations are dissolved and dispersoids are precipitated. The formed dispersoids hinder grain growth, but usually cannot increase the strength due to their coarse size of some 100 nm. Lower homogenisation temperatures should result in the precipitation of smaller dispersoids during homogenisation. The addition of Zr was investigated to increase this effect. Zr should form further dispersoids from the Al₃Zr phase. This requires a fundamental understanding of the temperature-dependent kinetics and the nature of precipitation formation during homogenisation. For this purpose, the as-cast state is first characterised via differential scanning calorimetry. Subsequently, a large number of homogenisation parameters are investigated and quantified via hardness testing. The micro- and nanostructure are investigated for promising parameters and a particle analysis is performed. In the present study, it was possible to precipitate fine dispersoids of few 10 nm by reducing the homogenisation temperature, which resulted in a significant increase in hardness. Alloying with Zr enabled the precipitation of further dispersoids with a size of a few nm in a high number density, which further increased the strength.

Keywords: AlMnMgSi alloy; EN AW-3105; homogenisation annealing; transmission electron microscopy (TEM); dispersoids; differential scanning calorimetry (DSC)



Citation: Broer, J.; Mallow, S.; Oldenburg, K.; Milkereit, B.; Kessler, O. The Influence of Homogenisation Parameters on the Microstructure and Hardness of AlMnFeMgSi(Zr) Wrought Alloys. *Metals* **2023**, *13*, 1706. <https://doi.org/10.3390/met13101706>

Academic Editor: Rebecca L. Higginson

Received: 29 August 2023

Revised: 28 September 2023

Accepted: 4 October 2023

Published: 7 October 2023



Copyright: © 2023 by the authors. Licensee MDPI, Basel, Switzerland. This article is an open access article distributed under the terms and conditions of the Creative Commons Attribution (CC BY) license (<https://creativecommons.org/licenses/by/4.0/>).

1. Introduction

After continuous casting, the conventional process chain of wrought aluminium alloys includes the steps of homogenisation annealing, hot forming and age hardening. Homogenisation is an important step in this process. The aim of homogenisation is to eliminate inhomogeneities and segregations from the casting process. In addition, dispersoids are formed from the supersaturated as-cast state, i.e., precipitates with a size typically below 1 µm. They hinder grain growth and thus ensure a small grain size. The microstructure development during homogenisation in 3xxx (AlMnFeMgSi) alloys has been described in the literature, especially the transformation behaviour of primary phases [1–3] and the precipitation behaviour of dispersoids [1,4]. During the homogenisation of 3xxx aluminium alloys, first, Mg/Si precursors form, and then they transform to the so-called “u-phase”, which finally act as nuclei for α-Al(Mn,Fe)Si dispersoid precipitation [5,6]. The dispersoids that form during conventional homogenisation, around 500 °C, are typically too large (some 100 nm) to increase the strength.

The precipitation of smaller dispersoids under modified homogenisation conditions has already been reported in the literature. It is shown that at lower homogenisation temperatures, a higher particle density and hardness can be achieved [7,8]. The dispersoids have a smaller size [4,7] and can increase the strength.

The purposeful adjustment of dispersoid size requires extensive knowledge of the precipitation behaviour of the dispersoids during homogenisation. Differential scanning calorimetry (DSC) is an established in situ method to characterise the precipitation and dissolution behaviour of particles in aluminium alloys [7,9–11]. DSC will be used to find a suitable temperature range for dispersoid precipitation. The heating rate to homogenisation temperature also plays a major role in the precipitation of fine dispersoids. Studies show that a low heating rate is essential to precipitate fine dispersoids in AlMnFeMgSi alloys [5,12].

The most common dispersoids in these alloys are of the α -Al(Mn,Fe)Si phase. Other dispersoid phases can be precipitated by adding further elements. Studies have demonstrated the positive influence of Zr and Sc on the mechanical properties of 3xxx [13], 5xxx [14,15] and 6xxx [16] aluminium alloys. It can be shown that Zr additionally increases the hardness [13–15]. In addition, it can be demonstrated that further fine dispersoids (size of a few nm) are formed [14–16].

The aim of this investigation is the precipitation of small dispersoids during homogenisation, which provide a strength-increasing effect through particle hardening. For this purpose, different homogenisation parameters are investigated and tested for hardness. In the case of promising parameter sets, the dispersoids are characterised using particle analysis.

2. Materials and Methods

2.1. Investigated Aluminium Alloys

For this purpose, two AlMnFeMgSi wrought alloys are investigated. They combine the microstructure features of 3xxx alloys (dispersoid precipitation during homogenisation) and 6xxx alloys (age hardening via the Mg₂Si sequence). Two aluminium alloys of the type EN AW-3105 (AlMn0.5Mg0.5) were investigated. One material was additionally alloyed with Zr. The additional alloying with Zr should enhance the dispersoid formation by including further dispersoid types. The chemical composition was analysed via optical emission spectroscopy (OES) and is shown in Table 1 with the nominal composition according to the European standard DIN EN 573-3 for these alloys. Samples were ground before OES analysis. OES analysis has typical detection limits in the ppm range. The material was direct-chill cast to ingots with a size of $\varnothing 100 \times 300$ mm. The melt was produced in a resistance-heated furnace with a SiC crucible.

Table 1. Mass fractions of the alloying elements in the investigated EN AW-3105 alloys and the nominal composition according to European standard DIN EN 573-3.

Alloy	Mass Fraction in %						
	Si	Fe	Cu	Mn	Mg	Ti	Zr
EN AW-3105	0.53	0.49	0.17	0.73	0.59	0.014	0.002
EN AW-3105 with Zr	0.55	0.46	0.17	0.73	0.58	0.016	0.195
DIN EN 573-3	≤ 0.6	≤ 0.7	≤ 0.3	0.3–0.8	0.2–0.8	≤ 0.1	≤ 0.05

2.2. Heat Treatments and Hardness Tests

First, linear heating experiments were performed in a DSC at a rate of 0.01 K s^{-1} to investigate the as-cast material (Figure 1a). The heating rate was chosen based on those that are typically used in industry. The heating experiments were performed in a SenSys Evo DSC (SETARAM, KEP TECHNOLOGIES SA, Mougins, France) with a sample size of $\varnothing 6 \times 21.65$ mm (mass ca. 1650 mg). The DSC experiments were carried out and evaluated using the method described by Kemsies et al. [7]. In addition, reheating experiments

after previous standard homogenisation were carried out to investigate the influence of prior homogenisation (Figure 1b). The standard homogenisation parameters, 550 °C for 24 h, were also chosen based on those that are typically used in industry. In this case, the previous homogenisation at 550 °C for 24 h was performed in the chamber furnace CWF 1100 (CARBOLITE GERO GmbH & Co. KG, Neuhausen, Germany), followed by air cooling. The samples were then frozen at −80 °C until DSC examination to preserve their condition.

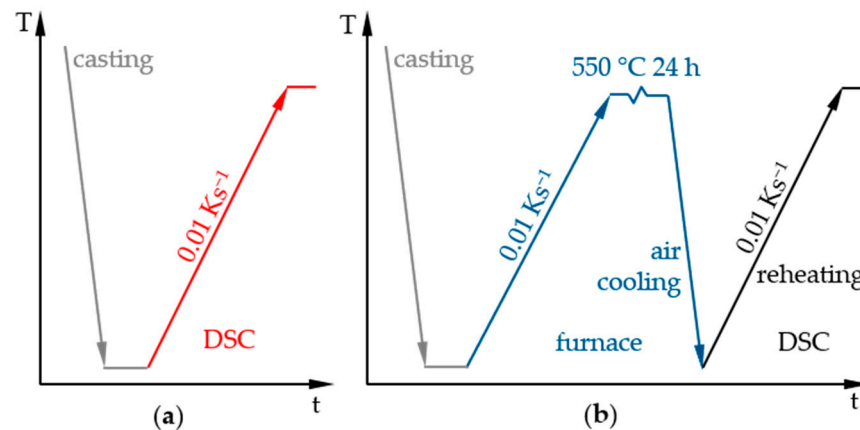


Figure 1. Time–temperature DSC programs for the (a) as-cast heating experiments and (b) reheating experiments after homogenisation at 550 °C for 24 h.

Next, different homogenisation parameters (Figure 2) were investigated to determine the effect on dispersoid precipitation. The heating rate was 0.01 Ks^{-1} for all homogenisation experiments. Kemsies [12] showed that a slow heating rate is necessary to form small dispersoids. Lodgaard et al. [5] also described that slow heating (ca. 0.05 Ks^{-1}) is required to achieve a high density of $\alpha\text{-Al}(\text{Mn,Fe})\text{Si}$ dispersoids. The homogenisation temperature varied from 370 to 460 °C in 30 K steps. This temperature range was selected based on DSC results according Figure 1. In addition, homogenisation at 550 °C was performed as a reference. The homogenisation duration ranged from 0 min (only heating to homogenisation temperature) up to 100 h and was finished with air cooling.

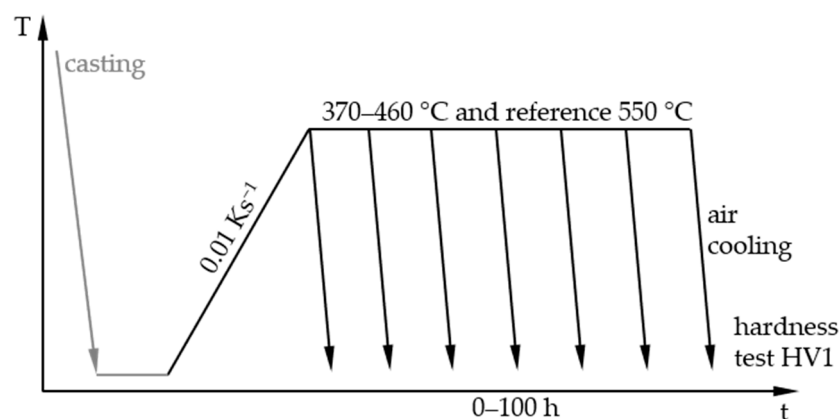


Figure 2. Time–temperature programs of homogenisation experiments.

Fresh as-cast samples ($\text{Ø}10 \times 2 \text{ mm}$) were used for all experiments. All samples of one temperature were heat-treated simultaneously in the furnace for all homogenisation durations and removed at the respective soaking times. The heat treatments were carried out in a CWF 1100 furnace (CARBOLITE GERO GmbH & Co. KG, Neuhausen, Germany). The samples were frozen at −80 °C after cooling to ensure the most similar intermediate storage at room temperature before hardness testing. For the hardness testing, six indentations were set on each specimen, from which the mean value was calculated. The hardness

tests were performed using the Vickers method HV1 on a hardness testing machine, KB 30 SR (HEGEWALD&PESCHKE MESS- UND PRÜFTECHNIK GmbH, Nossen, Germany).

The selected heat treatments were repeated with identical parameters on the $\text{Ø}3 \text{ mm} \times 20 \text{ mm}$ samples in a quenching dilatometer, Bähr 805A/D (TA INSTRUMENTS, New Castle, DE, USA), for transmission electron microscopy sample preparation.

2.3. Micro- and Nanostructure Analysis

Light microscopy (LM) specimens were prepared, finally polished with oxide polishing suspension (OPS) and then etched for 2 s according to WECK. The LM images were taken with the inverted reflected-light microscope LEICA DMI5000 M (LEICA Microsystems GmbH, Wetzlar, Germany). Data processing of the images was performed using the database-supported documentation and evaluation system, IMAGIC IMS (IMAGIC BILDVERARBEITUNG AG, Glattbrugg, Switzerland).

Scanning electron microscopy (SEM) samples were analysed using a field emission SEM MERLIN[®]VP Compact (CARL ZEISS AG, Oberkochen, Germany), equipped with an energy-dispersive X-ray (EDS) detector (XFlash 6/30) and the analysis software, Quantax400 (BRUKER Corp., Billerica, MA, USA). Representative areas of the samples were analysed and mapped to determine the elemental distribution on the basis of the EDS-spectra data using the QUANTAX ESPRIT microanalysis software (version 2.0; BRUKER Corp., Billerica, MA, USA). Embedded and polished samples were coated with 5 nm of carbon in a high-vacuum coating system, SAFEMATIC CCU-010 HV (SAFEMATIC GmbH, Zizers, Switzerland, for better conductivity, and were mounted on the SEM carrier with adhesive conductive carbon and aluminium tape (PLANO, Wetzlar, Germany). SEM-secondary electron (SEM-SE) images were obtained using a high efficiency Everhart-Thornley-type HE-SE detector at a 5 kV acceleration voltage. The acceleration voltage for the energy-dispersive X-ray (EDS) analysis was set to 15 kV.

For the transmission electron microscopy (TEM), a thin disk of about 350 μm thickness was cut from a $\text{Ø}3 \text{ mm}$ dilatometer sample using a diamond precision saw, ACCUTOM-10 (STRUERS GmbH, Willich, Germany). This disk was ground and polished to a thickness of about 80 μm . The final electrolytical thinning was carried out using a Tenupol 5 (STRUERS GmbH, Willich, Germany), operated at a temperature of about $-25 \text{ }^\circ\text{C}$ with a voltage of 9.5 V, using an electrolyte consisting of methanol and 53% nitric acid in a 2:1 ratio. TEM sample preselection was performed in a Talos L120C (THERMOFISHER SCIENTIFIC Inc., Waltham, MA, USA) device. The nanostructure of the homogenised samples was investigated in an analytical, probe aberration-corrected scanning transmission electron microscope (STEM), JEM-ARM200F NEOARM (JEOL Ltd., Akishima, Japan), equipped with a cold field emission gun operated at a 200 kV acceleration voltage. Images were acquired using a high-angle annular dark-field detector (HAADF), and the chemical composition of the relevant features were analysed using a EDS detector with an area of 100 mm^2 (JEOL Ltd., Akishima, Japan).

Particle analysis was performed on the HAADF-STEM images using the free data analysis software, Gwyddion (version 2.62) and IMAGIC IMS. For each material/state, 18 images with an area of ca. 1 μm^2 were analysed. The number of particles and the mean Feret diameter (mean diameter measured from 36 directions) were determined. The sample thickness was measured with a GATAN Continuum low-loss electron energy loss spectroscopy (ELLS) (GATAN Inc., Pleasanton, CA, USA) and the thickness was calculated according to Iakoubovskii's equation [17]. Table 2 shows the investigated sample volumes. Subsequently, the size distribution of the particles and the number density per μm^3 were calculated.

Table 2. Investigated sample volume of the particle analysis.

Alloy	EN AW-3105		EN AW-3105 with Zr	
State	460 °C 20 min	430 °C 1 h	460 °C 20 min	430 °C 1 h
analysed sample volume in μm^3	0.66	1.16	0.75	0.65

3. Results and Discussion

3.1. DSC Heating Curves of the As-Cast and Homogenised State

DSC heating investigations were carried out to understand the supersaturation and the precipitation kinetics of the material from the as-cast state. Figure 3 shows the DSC heating curves with a heating rate 0.01 K s^{-1} of both investigated alloys from the as-cast state (red curve) and after homogenisation at 550 °C for 24 h (black curve). The course of all four heating curves is similar. The DSC heating curves essentially show a sequence of exothermic and endothermic peaks. It should be noted that DSC always measures the sum signal, i.e., exothermic and endothermic reactions can overlap. During an exothermic peak, precipitation occurs (marked with lower case letters), whereas during endothermic reactions, dissolution occurs (marked with capital letters).

DSC-heating curves at 0.01 K s^{-1}
as-cast and after homogenisation at 550 °C 24 h

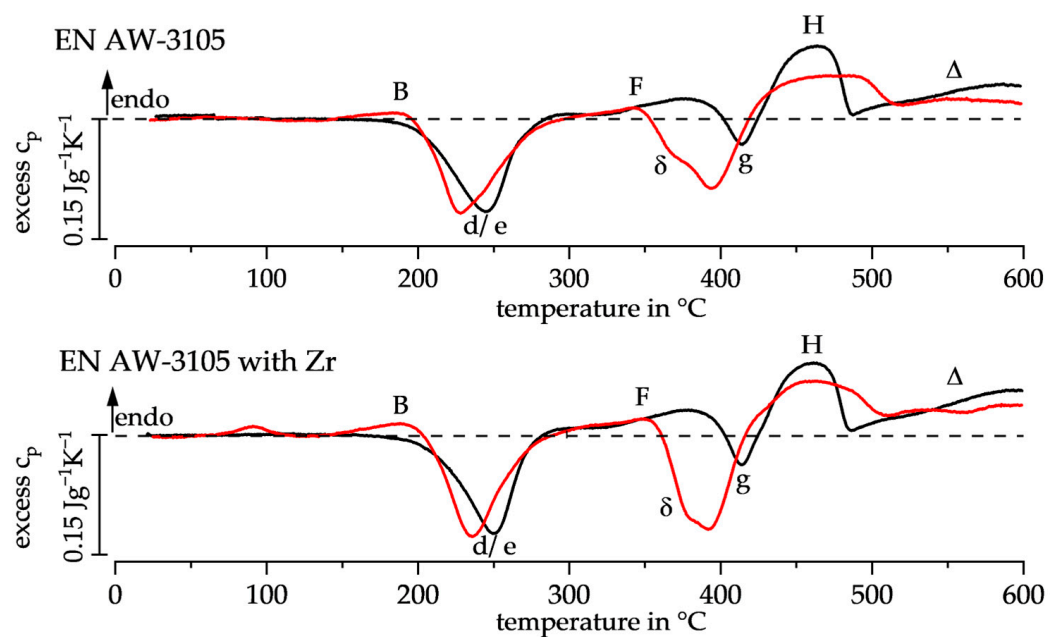


Figure 3. DSC heating curves for both alloys at 0.01 K s^{-1} from the as-cast state (red curve) and after homogenisation at 550 °C for 24 h (black curve).

The DSC heating curves of both investigated alloys are similar to those of AlMgSi (6xxx) alloys [9]. This can be explained by the relative high Si and Mg content of the EN AW-3105 alloy (Table 2). The peaks were assigned to the probable dissolution and precipitation steps of the $\beta\text{-Mg}_2\text{Si}$ sequence and of dispersoids, respectively, (Table 3) based on the literature.

Table 3. Dissolution and precipitation peaks and the assumed reactions in EN AW-3105. Peak designation according to Figure 3.

Peak	Dissolution Reaction	Precipitation Reaction
B	GP-zones [18]	
d/e		β'' /MgSiCu precursor [18]
F	β'' /MgSiCu precursor	
δ		α -Al(Mn,Fe)Si [5]
g		β -Mg ₂ Si [19]
H	β -Mg ₂ Si	
Δ	α -Al(Mn,Fe)Si [20]	

The DSC curves of the two alloys from the as-cast state are very similar and actually only differ in the overlapping ($\delta + g$) peak intensity at approximately 350–425 °C. The δ shoulder in the EN AW-3105 alloy with Zr seems to be more pronounced. Elasheri et al. [21] described that spherical Al₃Zr is precipitated at 300–450 °C. Thus, the larger peak ($\delta + g$) in the EN AW-3105 alloy with Zr could be due to the superimposed precipitation of the Al₃Zr phase.

Comparing the DSC curves after homogenisation (550 °C for 24 h) of the two alloys, no significant differences can be seen. But when comparing the as-cast and the homogenised state, clear differences can be found. Dissolution B is no longer visible in the curve from the homogenised state. The samples were reheated without intermediate room-temperature storage. Therefore, no GP-zones could form that would have been dissolved in peak B. The peak d/e shifts slightly to higher temperatures. An obvious difference is noticeable at the overlapping precipitation peak ($\delta + g$). In the homogenised state, only a weak exothermic peak (g) without a visible shoulder (δ) is detectable. Kemsies et al. [7] investigated a similar alloy, and concluded from conductivity measurements that the shoulder (δ) around 350 to 400 °C can be attributed to the precipitation of Mn-containing dispersoids. Lodgaard et al. [5] described that from 350 °C up to approximately 460 °C, dispersoids of the α -Al(Mn,Fe)Si phase form.

In both alloys and states, endothermic reactions are recognisable at high temperatures (>500 °C). In contrast, the typical DSC heating curves of 6xxx alloys [9] show reaction-free areas at temperatures above ca. 510 °C. Thus, the dissolution of the β -Mg₂Si phase should be completed at these temperatures. Li et al. [20] showed that Mn-containing dispersoids are further coarsened and partially dissolved at high temperatures up to 600 °C. This endothermic peak (Δ) can thus be associated with the coarsening and dissolution of the Mn-containing dispersoids.

The aim of the present research is to form many small dispersoids, which increase the strength. The homogenisation temperatures and homogenisation times were reduced and varied between 370 °C (approximate start of the shoulder, δ) and 430 °C (approximate end of the peak, g). Furthermore, we consider the integration of the solution annealing of Mg and Si into homogenisation. Accordingly, the precipitated β -Mg₂Si must be dissolved (Peak H). Therefore, 460 °C was chosen as an additional homogenisation temperature, as well as 550 °C as a reference temperature.

3.2. Hardness after Homogenisation

Figure 4 shows the hardness curves along the homogenisation duration at different temperatures for both alloys (Figure 4a for EN AW-3105 and Figure 4b for EN AW-3105 with Zr). EN AW-3105 in the as-cast state has a hardness of 68 HV1. The maximum hardness after homogenisation at the reference temperature (550 °C) of 46 HV1 is achieved directly after heating and decreases steadily to 42 HV1 after a 100 h soaking duration. The homogenisation at 460 °C also reaches the maximum hardness of 63 HV1 directly after heating. This shows up as a plateau, up to a soaking time of 20 min. Afterwards, the hardness decreases steadily to 49 HV1 up to 100 h. The hardness at the homogenisation temperature of 430 °C shows a plateau at 62 HV1, up to a soaking time of 3 h. Subsequently,

the hardness decreases steadily to 53 HV1 at 100 h. The hardness after homogenisation at 400 °C increases from 57 HV1 directly after heating to 64 HV1 after 10 h of soaking time. Following this, the hardness decreases to 54 HV1 at 100 h of holding time. The hardness at the lowest homogenisation temperature, 370 °C, increases with the rising soaking duration from 56 HV1 to 61 HV1 at 30 h, and then decreases slightly to 59 HV1.

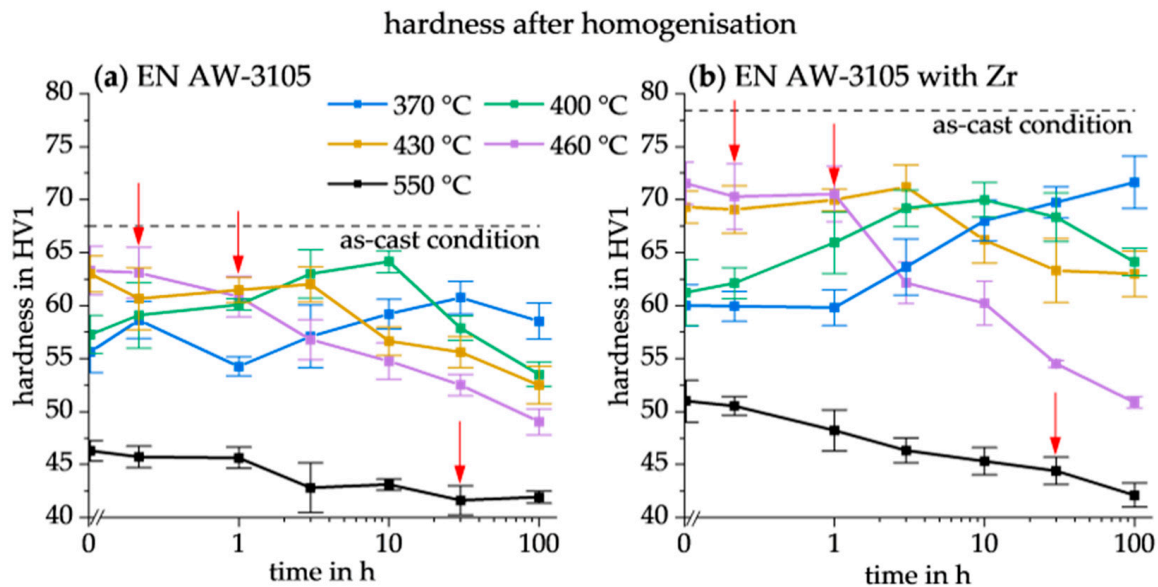


Figure 4. Hardness after homogenisation of (a) EN AW-3105 and (b) EN AW-3105 with Zr. Selected states for microstructure analysis are marked with arrows.

The hardness of the as-cast state of the EN AW-3105 alloy with Zr (Figure 4b) is 78 HV1. The general hardening behaviour of this alloy is similar to the EN AW-3105 alloy without Zr, but on a higher level. The maximum hardness of the reference temperature (550 °C) is 51 HV1 directly after reaching the homogenisation temperature, and decreases to 42 HV1 at 100 h. The hardness at a temperature of 460 °C remains at a plateau of about 71 HV1 from 0 to 1 h, and then falls to 51 HV1 at 100 h. The hardness at a temperature of 430 °C increases slightly from 69 to 71 HV1 at a duration of 3 h, and then decreases to 63 HV1 until 100 h. The hardness at a temperature of 400 °C rises from 61 to 70 HV1 at a homogenisation duration of 10 h, and then drops to 64 HV1 at 100 h. The hardness at a temperature of 370 °C shows a plateau of 60 HV1 from 0 to 1 h, and then rises to 72 HV1 up to 100 h. No decrease in hardness is noticeable in the investigated soaking time. The hardness curves of the different temperatures show a typical behaviour. The maximum hardness is reached earlier at higher temperatures due to the resulting faster diffusion.

Comparing the maximum hardness levels of the lower homogenisation temperatures of the EN AW-3105 alloy with the reference temperature of 550 °C shows an increase in hardness of about 39% (64 HV1 at 400 °C/10 h to 46 HV1) (Table 4). The EN AW-3105 alloy with Zr shows an increase of 39% (71 HV1 at 430 °C/3 h to 51 HV1) (Table 4).

Table 4. Maximum hardness levels of the respective homogenisation temperatures with the corresponding durations of the two investigated alloys.

Temperature	Duration	EN AW-3105	EN AW-3105 with Zr
		Hardness ± std	Hardness ± std
550 °C	0 h	46 ± 1 HV1	51 ± 2 HV1
460 °C	0.33 h	63 ± 2 HV1	70 ± 3 HV1
430 °C	3 h	62 ± 2 HV1	71 ± 2 HV1
400 °C	10 h	64 ± 1 HV1	70 ± 2 HV1
370 °C	30 h	61 ± 2 HV1	70 ± 1 HV1

All hardness values after homogenisation are below the hardness of the as-cast states. This is probably due to the reduced supersaturation and coarsened precipitates. It is clear from the DSC heating curves (Figure 3) that at least the coarse β -Mg₂Si-phase is additionally precipitated at the selected temperatures (peak g). Two homogenisation parameters were selected for further microstructure analysis. The parameters of 460 °C for 20 min and 430 °C for 1 h were chosen from their relative high hardness. These parameters have the further advantage that after these soaking times, no immediate hardness decrease occurs, i.e., these dispersoids are in a relatively stable condition regarding further heat treatments.

3.3. Microstructure of the Alloys in As-Cast and Homogenised State

3.3.1. Light Microscopy and SEM Analysis

Light microscopy images were taken of the selected conditions to assess the microstructure after homogenisation. Figure 5 shows the etched microstructure in the LM of both alloys in different states. The microstructure of EN AW-3105 in the as-cast state (Figure 5a) shows a dendritic microstructure of aluminium solid solution with a dark grey, Chinese script-shaped, interdendritic eutectic (marked as I). Inside the eutectic, the elements Al, Si, Fe and Mn were revealed in the SEM via EDS (see Figure 6). The eutectic probably contains primary particles of the α -Al(Mn,Fe)Si phase.

In addition, bluish precipitates (marked as II) are visible. These particles contain Mg, Si and sometimes Cu (revealed in SEM-EDS, see Figure 6) and are likely to be primary β -Mg₂Si or Q-MgSiCu.

The EN AW-3105 alloy with Zr (Figure 5b) in the as-cast state shows a similar microstructure with additional, sporadic, grey precipitates, with a length of approximately 20 μ m (marked as III). These particles contain Zr, Si and Ti (see Figure 7). These are possibly primary phases of Al₃Zr. Obviously, Zr is not completely in a supersaturated solid solution in the as-cast state. But the enhanced hardening behaviour in Figure 4 proves that at least a certain amount of Zr is effective in dispersoid formation.

Figure 5c,d show the microstructure of both alloys after homogenisation at 550 °C for 24 h. The Chinese script-shaped eutectic (I) is still visible but appears more compact and remodelled. No bluish precipitates occur, i.e., all primary β -Mg₂Si or Q-MgSiCu phases were dissolved during homogenisation. Within the dendrites, many small particles (marked as IV) are obvious. In the light microscope images, these particles tend to be shown larger due to etching. SEM examinations (see Figure 8) show that these particles are a few 100 nm in size and EDS shows that they contain Mn and Si (see Figure 9). Thus, it is likely that these are dispersoids of type α -Al(Mn,Fe)Si. No differences can be seen between the two alloys in the light microscope images.

After homogenisation at 460 °C for 20 min (Figure 5e,f), it can be seen that the Chinese script-shaped eutectic (I) is more pronounced and was only slightly remodelled at the lower homogenisation temperature. Plus, some bluish precipitates (II) are recognisable. These Mg- and Si-containing particles (II) are primary β -Mg₂Si particles that were not dissolved during homogenisation. A comparison with the DSC heating curves (Figure 3) shows that the β -Mg₂Si phase is not completely dissolved during homogenisation at 460 °C. The inhomogeneous etching behaviour within the α -dendrites in this condition (460 °C for 20 min) is different from the as-cast condition ((a) and (b)). This could be an indication of fine dispersoids (IV). There is no noticeable difference between the two alloys.

The microstructure after homogenisation at 430 °C for 1 h (Figure 5g,h) also shows a pronounced Chinese script-shaped eutectic (I) similar to after homogenisation at 460 °C for 20 min. In addition, some bluish precipitates (II) are also visible here. The etching inside the dendrites also shows a different behaviour than that of the as-cast state, which could indicate fine dispersoids (IV). There is no significant difference between the two alloys after this homogenisation.

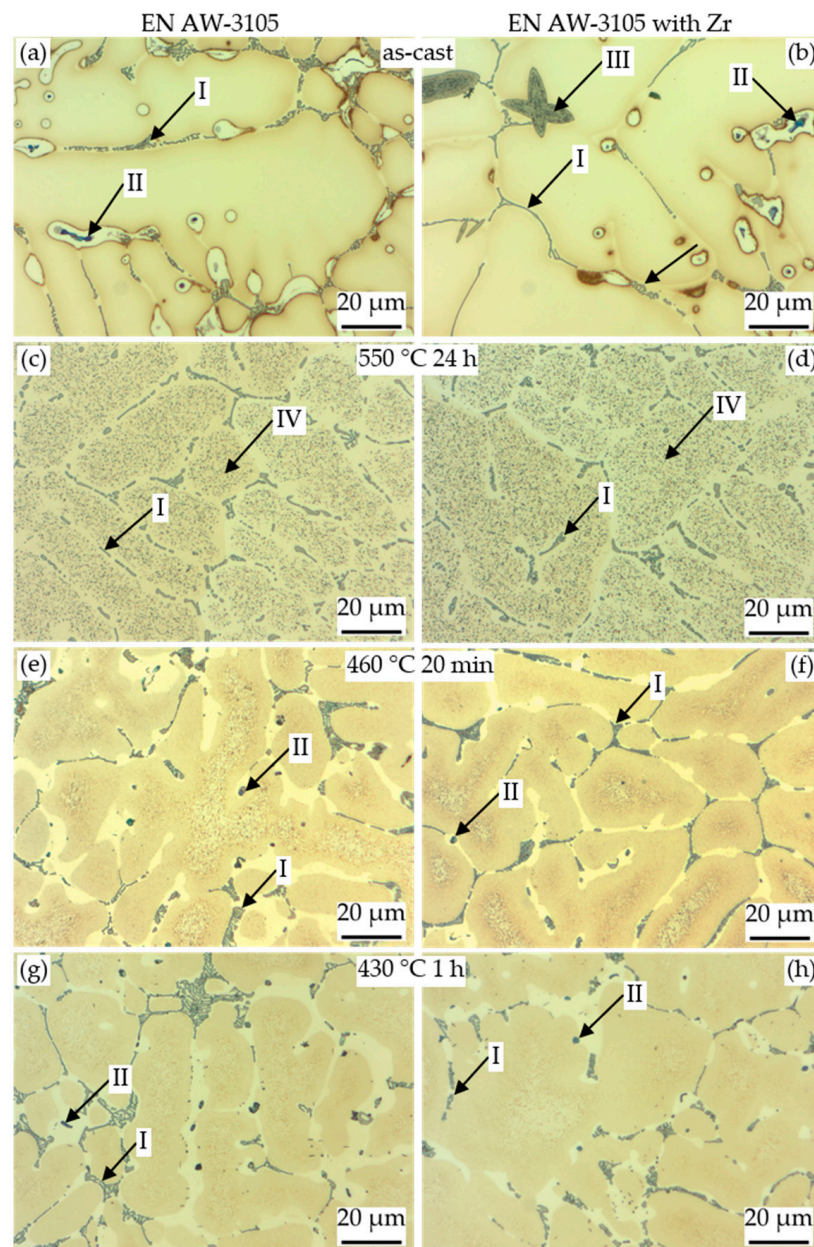


Figure 5. Light microscopic images of the WECK-etched alloys, EN AW-3105 and EN AW-3105 with Zr, in the as-cast (a,b), homogenised at 550 °C for 24 h (c,d), homogenised at 460 °C for 20 min (e,f) and homogenised at 430 °C for 1 h (g,h) states. Particle types I to IV are described in the text.

The SEM images show additional particles (marked as V) after homogenisation at 460 °C for 20 min as well as at 430 °C for 1 h (Figure 10). These particles are rod-shaped, about 1 μm in length, and appear perpendicular to each other inside one α -grain. They contain Mg and Si (revealed in the SEM-EDS, see Figure 11). These particles are probably secondary β or β' and precipitate during slow heating to homogenisation temperature (compare with Figure 3). Table 5 summarizes the different observed particle types.

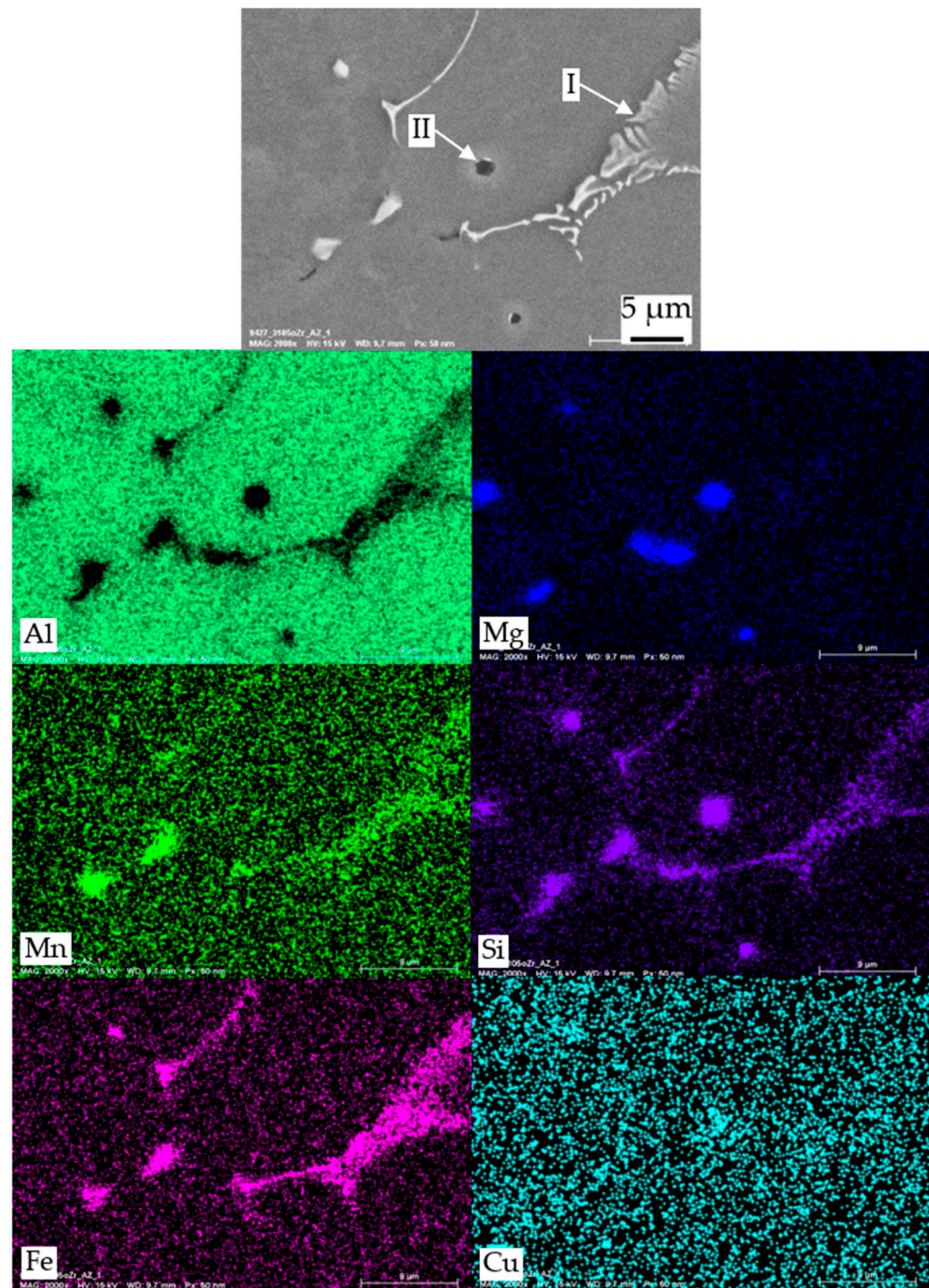


Figure 6. SEM-EDS mapping of the EN AW-3105 alloy (particle types I and II) in the as-cast state. Particle types I and II are described in the text.

Homogenisation at 460 °C for 20 min as well as at 430 °C for 1 h eliminated the segregations and the inhomogeneity of the as-cast microstructure to a lesser extent than homogenisation at 550 °C for 24 h. However, the hardening behaviour (Figure 4) showed an increased strength with the fine dispersoids. The influence of these two superimposing but opposite effects on mechanical properties must be further studied through detailed mechanical testing, e.g., tensile and fatigue tests. A subsequent hot forming of these wrought aluminium alloys after homogenisation may further reduce the segregations and inhomogeneities of the microstructure.

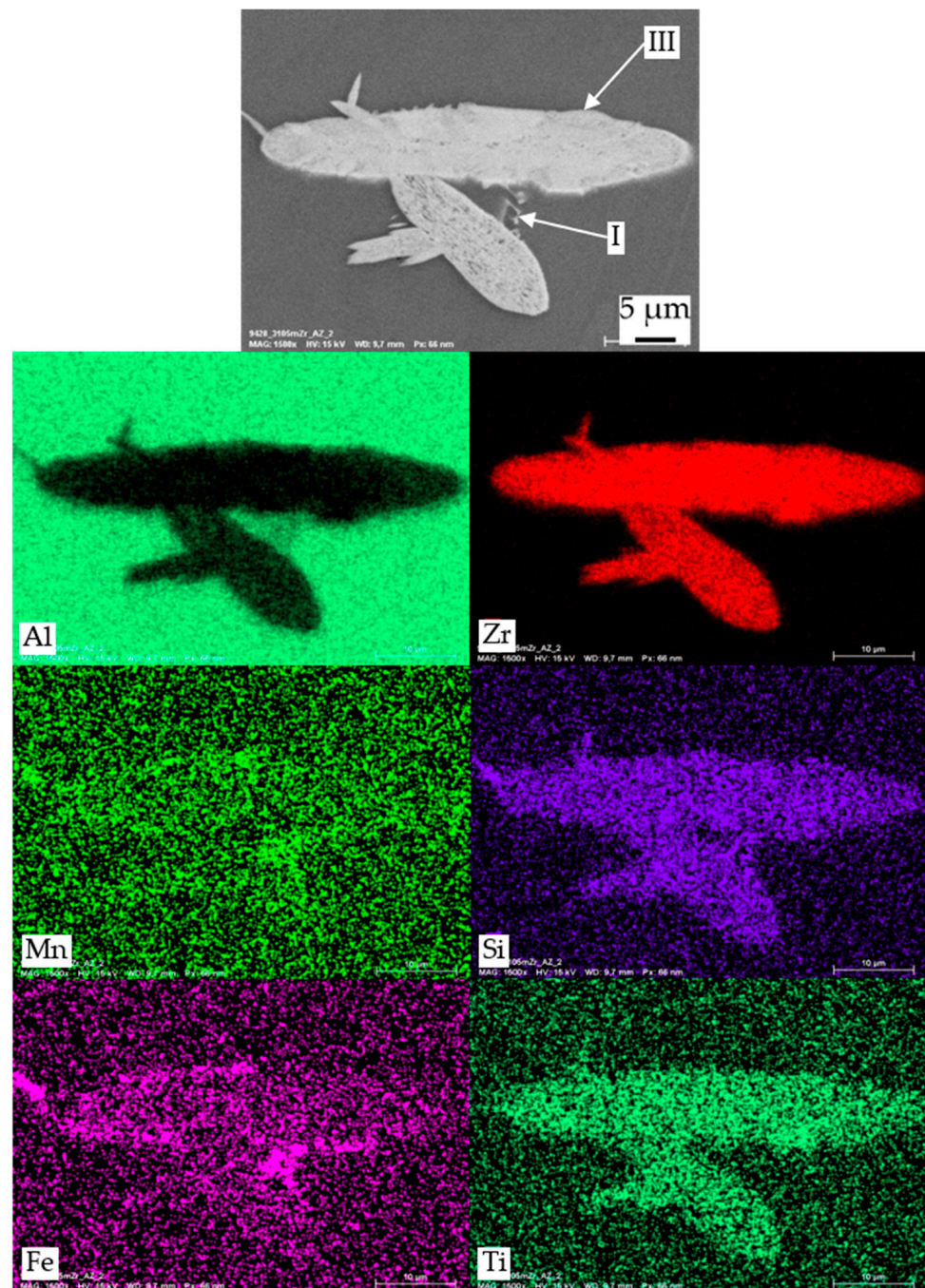


Figure 7. SEM-EDS mapping of the EN AW-3105 alloy with Zr (particle type III) in the as-cast state. Particle types I and III are described in the text.

3.3.2. TEM Analysis

TEM images were taken in order to make a quantified statement on the particle sizes. Different particle types that were found in the TEM images can be seen in Figure 12. A distinction is made between four particle types according to their morphology. Type IV-1 are roundish particles with a diameter of 30–100 nm. The EDS revealed that these particles contain Mn and Si. Type IV-2 are elongated particles with a length of 30–100 nm and a thickness of approximately 20 nm. These particles also contain Mn and Si. Possibly, these two particle types are the same particles viewed from different directions.

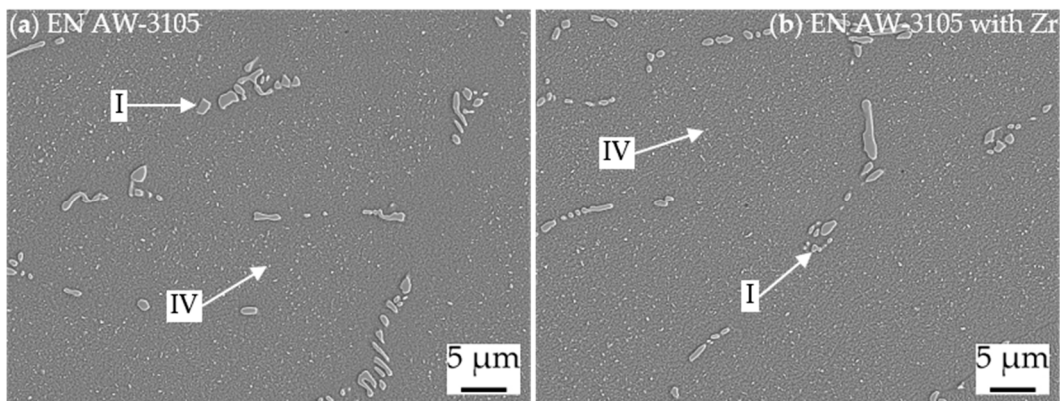


Figure 8. SEM images of the etched alloys, (a) EN AW-3105 and (b) EN AW-3105 with Zr, after homogenisation at 550 °C for 24 h. Particle types I and IV are described in the text.

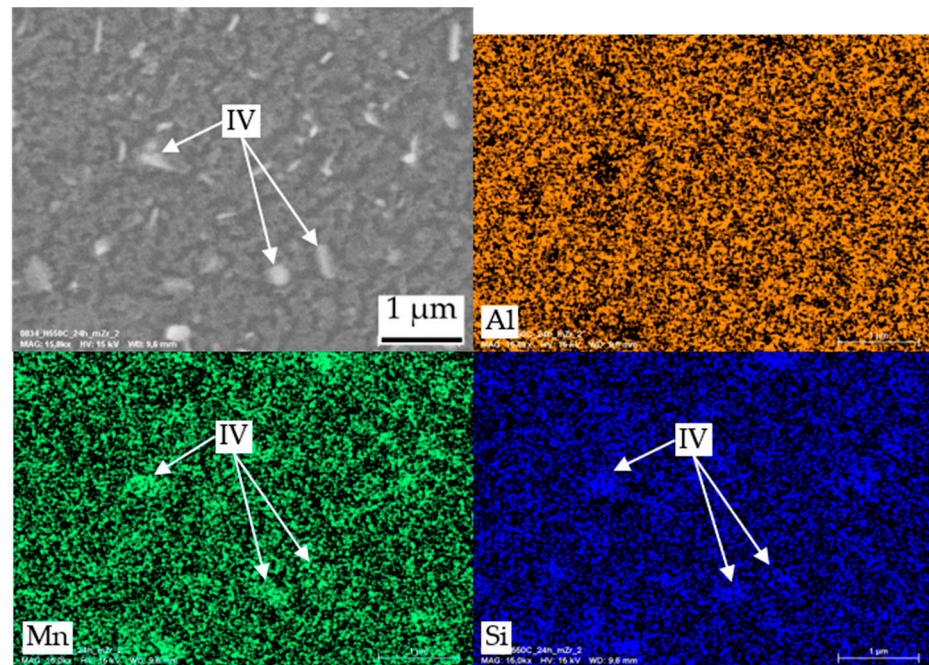


Figure 9. SEM-EDS mapping of the etched EN AW-3105 alloy with Zr (particle type IV) after homogenisation at 550 °C for 24 h. Particle type IV is described in the text.

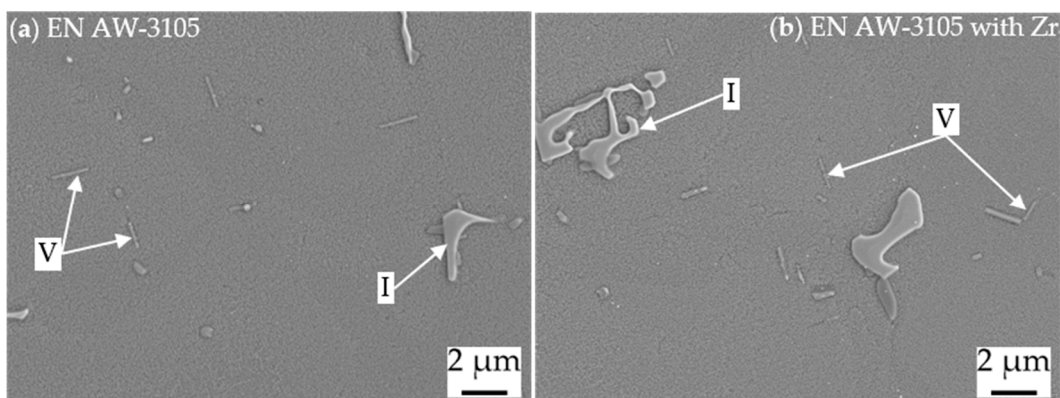


Figure 10. SEM images of the etched alloys, (a) EN AW-3105 and (b) EN AW-3105 with Zr, after homogenisation at 430 °C for 1 h. Particle types I and V are described in the text.

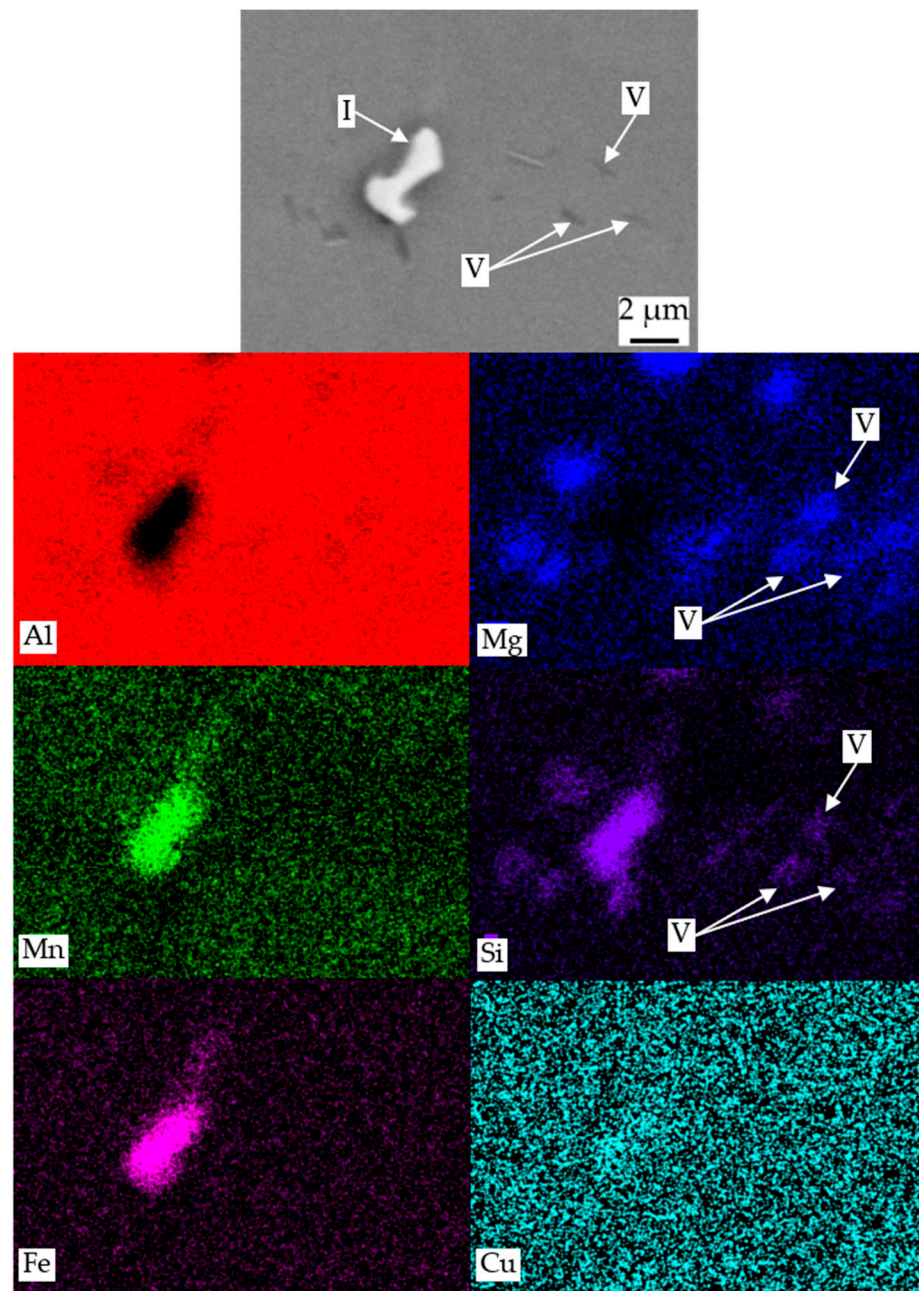


Figure 11. SEM-EDS mapping of the etched EN AW-3105 alloy with Zr (particle type V) after homogenisation at 430 °C for 1 h. Particle types I and V are described in the text.

Table 5. Contained elements according to the EDS SEM analysis of the visible phases in the microstructure.

Particle Type	Contained Elements	Assumed Phase
I	Al, Mn, Si, Fe	primary α -Al(Mn,Fe)Si
II	Mg, Si, (Cu)	primary β -Mg ₂ Si or Q-MgSiCu
III	Zr, Si, Ti, (Al)	primary Al ₃ Zr
IV	Mn, Si	dispersoids α -Al(Mn,Fe)Si
V	Mg, Si	secondary β or β' [22]

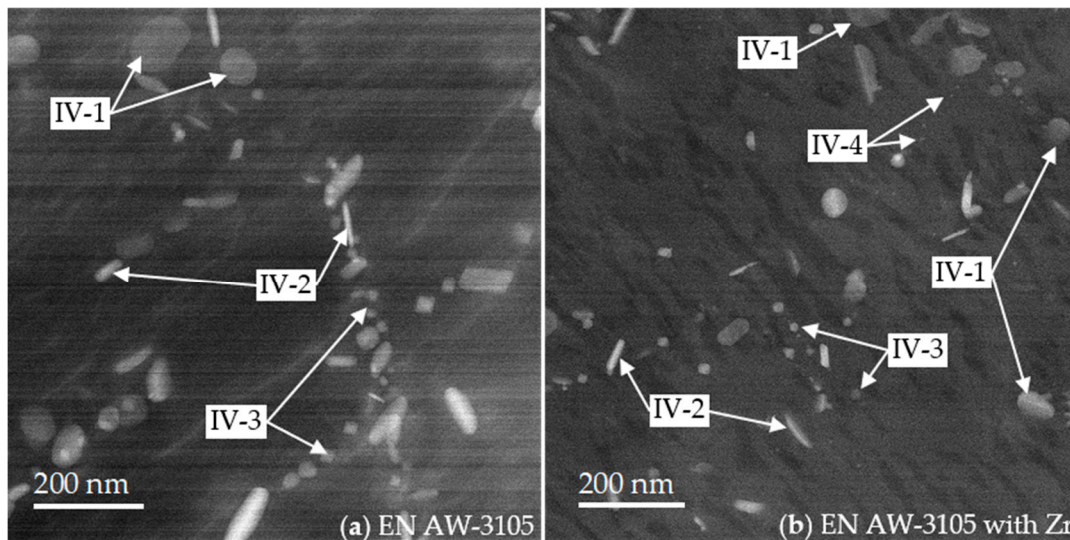


Figure 12. Dispersoid types found in alloys (a) EN AW-3105 and (b) EN AW-3105 with Zr after homogenisation at 430 °C for 1 h. Particle types IV-1 to IV-4 are described in the text.

Other particles were found, such as medium-sized round particles with a diameter of 10–30 nm (type IV-3); these particles also contain Mn and Si. The last type of particles (IV-4) were only detected in the EN AW-3105 alloy with Zr. These small, round particles, with a diameter of 5–10 nm, contain Zr, according to the EDS.

Figure 13 shows the frequencies of the Feret diameters of the dispersoids (all types IV-1 to IV-4, not distinguished) of both investigated alloys at the two homogenisation parameters, 460 °C for 20 min and 430 °C for 1 h. The most common particle size in the EN AW-3105 alloy is between 15 and 20 nm. The differences in particle distribution between the two homogenisation conditions are small (Table 6).

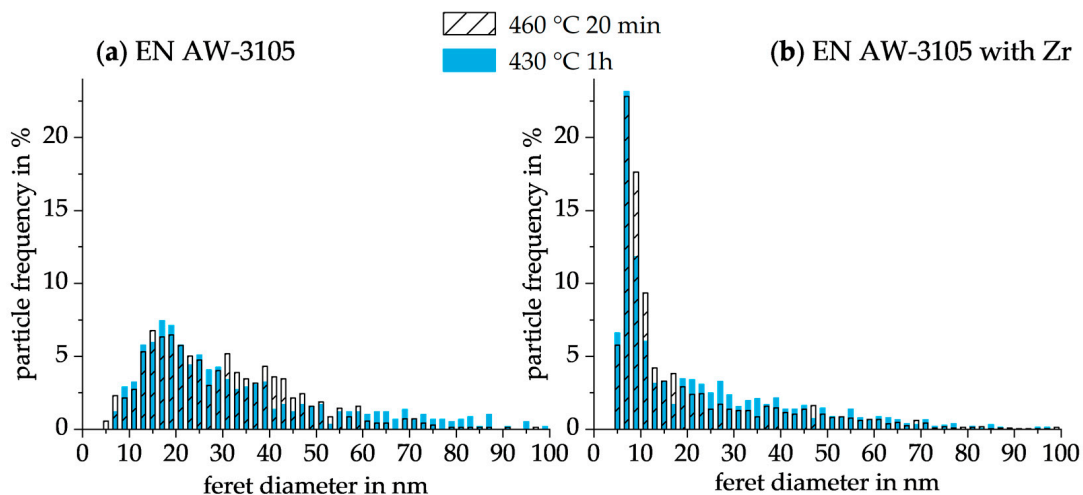


Figure 13. Dispersoid size distribution of EN AW-3105 (a) and EN AW-3105 with Zr (b) after homogenisation at 460 °C for 20 min (black) and 430 °C for 1 h (blue).

The particle distribution of the EN AW-3105 alloy with Zr is very different compared to the EN AW-3105 alloy without Zr. The most frequent particle size in this alloy is between 5 and 10 nm. The proportion of very small (<10 nm) particles is approximately 42% (430 °C for 1 h) and 46% (460 °C for 20 min) of the evaluated particles for the respective homogenisation state. This is achieved due to the small Zr-containing particles (Type V-4) seen in the TEM images (Figure 12). Again, the differences in particle distribution between the two homogenisation conditions are small (Table 6).

Table 6. Classification of the particle sizes into groups of different homogenised states.

Ferret Diameter in nm	Sum of Frequency in %			
	EN AW-3105		EN AW-3105 with Zr	
	430 °C 1 h	460 °C 20 min	430 °C 1 h	460 °C 20 min
<10	4.1	5.0	42.6	46.2
10–30	49.8	50.0	32.1	32.8
30–60	28.3	39.7	20.4	16.4
>60	17.8	5.3	4.9	4.6

In the EN AW-3105 alloy with Zr, the number density per μm^3 is significantly higher than in the EN AW-3105 alloy (Table 7). Thus, significantly smaller and significantly more particles are formed. It can be assumed that additional dispersoids (probably Al_3Zr) are formed. This correlates very well with the improved hardening behaviour (Figure 4).

Table 7. Number density of dispersoids after different homogenisations.

Alloy State	EN AW-3105		EN AW-3105 with Zr	
	460 °C 20 min	430 °C 1 h	460 °C 20 min	430 °C 1 h
Number density per μm^3	1057	505	2783	2348

The previous results show that an increase in strength during homogenisation is possible with lower annealing temperatures. Additional alloying with Zr seems to make a further positive contribution. It should be checked whether this beneficial strength contribution of the dispersoids can be maintained in the subsequent process chain, including hot forming. Furthermore, the grain size must be investigated along the whole process chain to see if smaller dispersoids can hinder grain growth to the same extent as conventional coarser dispersoids. Wong et al. [23] described that additional alloying with Zr reduced the grain size in an AlMgSi alloy. Finally, a further strength increase through precipitation hardening via the $\beta\text{-Mg}_2\text{Si}$ sequence may be superimposed.

4. Conclusions

An approach for improving dispersoid hardening in wrought AlMnFeMgSi(Zr) alloys was investigated. The relevant temperature range for dispersoid precipitation was determined using DSC and set to 370–460 °C. It could be shown that the hardness after homogenisation with lower homogenisation temperatures could be increased by approximately 40% compared to the reference homogenisation at 550 °C: 64 HV1 at 400 °C/10 h vs. 46 HV1 for the EN AW-3105 alloy and 71 HV1 at 430 °C/3 h vs. 51 HV1 for the EN AW-3105 alloy with Zr.

In the TEM images, fine particles with different shapes and a main diameter of 15–20 nm could be identified. The element analyses suggested dispersoids of the $\alpha\text{-Al(Mn,Fe)Si}$ phase. Furthermore, the addition of dispersoid former Zr results in many small (5–10 nm) dispersoids (probably Al_3Zr) with a high number density, which had a positive influence on the hardness.

Author Contributions: Conceptualization, J.B., B.M. and O.K.; investigation, J.B., S.M. and K.O.; writing—original draft preparation, J.B.; writing—review and editing, O.K.; visualization, J.B.; supervision, O.K.; funding acquisition, O.K. All authors have read and agreed to the published version of the manuscript.

Funding: This research was funded by the German Research Foundation (DFG), within the scope of the research project “Superimposed Dispersoid Hardening and Age Hardening of Aluminium Alloys” (DFG KE616/32-1, AOBJ 672438). We also acknowledge the German Research Foundation (DFG) for funding the transmission electron microscopes Jeol JEM-ARM200F NEOARM STEM (DFG INST 264/161-1 FUGG, AOBJ 643044) and ThermoFisher Talos L120C (DFG INST 264/188-1 FUGG, AOBJ 672500).

Data Availability Statement: Data available on request.

Acknowledgments: The authors also thank the Electron Microscopy Centre (EMC) of University Medicine Rostock for the use of the SEM.

Conflicts of Interest: The authors declare no conflict of interest.

References

1. Sun, D.L.; Kang, S.B.; Koo, H.S. Characteristics of morphology and crystal structure of α -phase in two Al-Mn-Mg alloys. *Mater. Chem. Phys.* **2000**, *63*, 37–43. [CrossRef]
2. Li, Y.; Arnberg, L. Evolution of eutectic intermetallic particles in DC-cast AA3003 alloy during heating and homogenization. *Mater. Sci. Eng. A* **2003**, *347*, 130–135. [CrossRef]
3. Alexander, D.; Greer, A.L. Solid-state intermetallic phase transformations in 3XXX aluminium alloys. *Acta Mater.* **2002**, *50*, 2571–2583. [CrossRef]
4. Pettersen, T.; Li, Y.J.; Furu, T.; Marthinsen, K. Effect of Changing Homogenization Treatment on the Particle Structure in Mn-Containing Aluminium Alloys. *Mater. Sci. Forum* **2007**, *558–559*, 301–306. [CrossRef]
5. Li, Z.; Zhang, Z.; Chen, X.-G. Effect of Metastable Mg₂Si and Dislocations on α -Al(MnFe)Si Dispersoid Formation in Al-Mn-Mg 3xxx Alloys. *Met. Mater. Trans. A* **2018**, *49*, 5799–5814. [CrossRef]
6. Lodgaard, L.; Ryum, N. Precipitation of dispersoids containing Mn and/or Cr in Al-Mg-Si alloys. *Mater. Sci. Eng. A* **2000**, *283*, 144–152. [CrossRef]
7. Kemsies, R.H.; Milkereit, B.; Wenner, S.; Holmestad, R.; Kessler, O. In situ DSC investigation into the kinetics and microstructure of dispersoid formation in Al-Mn-Fe-Si(-Mg) alloys. *Mater. Des.* **2018**, *146*, 96–107. [CrossRef]
8. Pettersen, T.; Furu, T.; Håkonsen, A. Effect of Changing Homogenisation Treatment for the Alloys AA3102 and AA3103. *Mater. Sci. Forum* **2002**, *396–402*, 1067–1072. [CrossRef]
9. Osten, J.; Milkereit, B.; Schick, C.; Kessler, O. Dissolution and precipitation behaviour during continuous heating of Al-Mg-Si alloys in a wide range of heating rates. *Materials* **2015**, *8*, 2830–2848. [CrossRef]
10. Fröck, H.; Reich, M.; Milkereit, B.; Kessler, O. Scanning rate extension of conventional DSCs through indirect measurements. *Materials* **2019**, *12*, 1085. [CrossRef]
11. Milkereit, B.; Österreich, M.; Schuster, P.; Kirov, G.; Mukeli, E.; Kessler, O. Dissolution and Precipitation Behavior for Hot Forming of 7021 and 7075 Aluminum Alloys. *Metals* **2018**, *8*, 531. [CrossRef]
12. Kemsies, R.H. Dispersoidbildung und Dispersoidstabilität in Aluminium-Mangan-Legierungen. Ph.D. Thesis, Rostock University, Rostock, Germany, 2019. Available online: https://rosdok.uni-rostock.de/resolve/id/rosdok_disshab_0000002154 (accessed on 27 August 2023).
13. Vlach, M.; Stulíková, I.; Smola, B.; Kudrnova, H.; Kekule, T.; Malek, J.; Ocenasek, V. Phase Transformations and Recrystallization in Cold-Rolled Al-Mn, Al-Sc-Zr and Al-Mn-Sc-Zr Alloy. *Defect Diffus. Forum* **2014**, *354*, 93–100. [CrossRef]
14. Algendy, A.Y.; Liu, K.; Rometsch, P.; Parson, N.; Chen, X.-G. Effect of Sc and Zr Additions on Dispersoid Microstructure and Mechanical Properties of Hot-Rolled AA5083. In *Light Metals 2023*; Broek, S., Ed.; Springer Nature Switzerland: Cham, Switzerland, 2023; pp. 1229–1237, ISBN 978-3-031-22531-4.
15. Pan, S.; Wang, Z.; Li, C.; Wan, D.; Chen, X.; Chen, K.; Li, Y. Achieving superior dispersion-strengthening effect in an AA5xxx Al-Mg-Mn alloy by micro-alloying. *Mater. Des.* **2023**, *226*, 111647. [CrossRef]
16. Elasheri, A.; Elgallad, E.M.; Parson, N.; Chen, X.-G. Evolution of Zr-Bearing Dispersoids during Homogenization and Their Effects on Hot Deformation and Recrystallization Resistance in Al-0.8%Mg-1.0%Si Alloy. *J. Mater. Eng. Perform.* **2021**, *30*, 7851–7862. [CrossRef]
17. Iakoubovskii, K.; Mitsuishi, K.; Nakayama, Y.; Furuya, K. Thickness measurements with electron energy loss spectroscopy. *Microsc. Res. Tech.* **2008**, *71*, 626–631. [CrossRef] [PubMed]
18. Barbosa, C.; Rebello, J.M.A.; Acselrad, O.; Dille, J.; Delplancke, J.L. Identification of Precipitates in 6013 Aluminum Alloy (Al-Mg-Si-Cu). *Z. Met.* **2002**, *93*, 208–211. [CrossRef]
19. Ohmori, Y.; Doan, L.C.; Matsuura, Y.; Kobayashi, S.; Nakai, K. Morphology and Crystallography of β -Mg₂Si Precipitation in Al-Mg-Si Alloys. *Mater. Trans.* **2001**, *42*, 2576–2583. [CrossRef]
20. Li, Y.; Arnberg, L. Quantitative study on the precipitation behavior of dispersoids in DC-cast AA3003 alloy during heating and homogenization. *Acta Mater.* **2003**, *51*, 3415–3428. [CrossRef]
21. Elasheri, A.; Elgallad, E.M.; Parson, N.; Chen, X.-G. Nucleation and transformation of Zr-bearing dispersoids in Al-Mg-Si 6xxx alloys. *J. Mater. Res.* **2023**, *38*, 696–707. [CrossRef]

22. Lypchanskyi, O.; Rigas, N.; Korpała, G.; Merklein, M.; Prah, U. Ex-situ and in-situ investigations of the microstructural evolution of AA6082 aluminum alloy during heat treatment. *Mater. Sci. Eng. A* **2023**, *870*, 144828. [[CrossRef](#)]
23. Wong, K.M.; Daud, A.R.; Jalar, A. Microhardness and Tensile Properties of a 6XXX Alloy Through Minor Additions of Zr. *J. Mater. Eng. Perform.* **2009**, *18*, 62–65. [[CrossRef](#)]

Disclaimer/Publisher’s Note: The statements, opinions and data contained in all publications are solely those of the individual author(s) and contributor(s) and not of MDPI and/or the editor(s). MDPI and/or the editor(s) disclaim responsibility for any injury to people or property resulting from any ideas, methods, instructions or products referred to in the content.